

Magnesium isotopes: a tool to understand self-enrichment in Globular Clusters

P. Ventura¹, F. D’Antona¹, G. Imbriani², M. Di Criscienzo¹, F. Dell’Agli^{3,4},
M. Tailo⁵

¹*INAF – Osservatorio Astronomico di Roma, Via Frascati 33, 00078, Monte Porzio Catone (RM), Italy*

²*Dipartimento di Scienze Fisiche, Università di Napoli Federico II, Italy*

³*Instituto de Astrofísica de Canarias, E-38205 La Laguna, Tenerife, Spain*

⁴*Departamento de Astrofísica, Universidad de La Laguna (ULL), E-38206 La Laguna, Tenerife, Spain*

⁵*Dipartimento di Fisica, Università degli Studi di Cagliari, SP Monserrato-Sestu km 0.7, I-09042 Monserrato, Italy*

Accepted, Received; in original form

ABSTRACT

A critical issue in the asymptotic giant branch (AGB) self-enrichment scenario for the formation of multiple populations in Globular Clusters (GCs) is the inability to reproduce the magnesium isotopic ratios, despite the model in principle can account for the depletion of magnesium. In this work we analyze how the uncertainties on the various p-capture cross sections affect the results related to the magnesium content of the ejecta of AGB stars. The observed distribution of the magnesium isotopes and of the overall Mg-Al trend in M13 and NGC 6752 are successfully reproduced when the proton-capture rate by ^{25}Mg at the temperatures ~ 100 MK, in particular the $^{25}\text{Mg}(p, \gamma)^{26}\text{Al}^m$ channel, is enhanced by a factor ~ 3 with respect to the most recent experimental determinations. This assumption also allows to reproduce the full extent of the Mg spread and the Mg-Si anticorrelation observed in NGC 2419. The uncertainties in the rate of the $^{25}\text{Mg}(p, \gamma)^{26}\text{Al}^m$ reaction at the temperatures of interest here leave space for our assumption and we suggest that new experimental measurements are needed to settle this problem. We also discuss the competitive model based on the super massive star nucleosynthesis.

Key words: Stars: abundances – Stars: AGB and post-AGB – Stars: carbon – Globular Clusters: general

1 INTRODUCTION

The research focused on Globular Clusters received a boost in the last decades, owing to results from high resolution spectroscopy, photometry and spectrophotometry, which have challenged the traditional paradigm that GCs are simple stellar populations.

On the spectroscopic side, practically all the GCs of the Milky way so far examined present star-to-star variations, which trace well defined abundance patterns, such as the C-N and O-Na anti-correlations, whose extension varies from cluster to cluster (Gratton et al. 2012). These abundance variations were observed also at the surface of unevolved stars (e.g. Gratton et al. 2001); for these stars, unlike red giants, the effects of any possible ‘in situ’ production mechanism can be disregarded. This discovery led to the conclusion that in GCs a variety of generations of stars coexist, each characterized by a different chemical composition.

On the photometric side, a great step forward towards the identification of multiple stellar generations was taken

when the presence of a “blue main sequence” was discovered in ω Centauri (Bedin et al. 2004) and in NGC 2808 (Piotto et al. 2007), requiring the presence of a group of stars formed with a helium content much larger than the standard Big Bang abundance. The blue main sequences confirmed early predictions, based on the analysis of the complex morphology of the horizontal branch (HB) of some GCs (D’Antona et al. 2002; D’Antona & Caloi 2004). In NGC 2808, three groups of stars differing in their helium were shown to coexist, with helium mass fractions ranging from the primordial, $Y \simeq 0.25$ up to $Y \lesssim 0.40$ (D’Antona et al. 2005; Piotto et al. 2007). Conversely, in other GCs, such as 47 Tuc, only a very modest spread of helium is required to reproduce the width of the main sequence (MS) and the morphology of the HB (Di Criscienzo et al. 2010).

The Hubble Space Telescope (HST) UV Legacy Survey (Piotto et al. 2015) has recently exploited the sensitivity of UV photometric observations to different molecular bands, to disentangle the stellar populations in 57 GCs. This project allowed to sort out the different stellar components

present in each GC, providing a valuable tool to understand how multiple populations formed and evolved in Galactic GCs.

The combination of the spectroscopic and spectrophotometric evidences collected so far indicate that in GCs, after the formation of the first generation (FG), a second generation (SG) of stars formed, from gas contaminated by p-capture nucleosynthesis. Several star formation events may contribute to different SG groups (Milone et al. 2017).

Until now 4 main classes of polluters have been proposed, namely (in order of decreasing mass): super-massive main sequence stars (Denissenkov & Hartwick 2014); fast rotating massive stars (Decressin et al. 2007; Krause et al. 2013), massive binaries (De Mink et al. 2009) and massive AGB stars (D’Ercole et al. 2008). In all models, the proton capture reactions, producing the peculiar abundances found in the SG stars, occur in the convective hydrogen burning core; the only exception is the AGB case, where the site of nucleosynthesis is the bottom of the deep convective envelope (hot bottom burning, HBB). All the proposed scenarios have been subject to heavy criticism, in particular concerning the mass budget issue (see, e.g. Renzini et al. 2015), so that the most recent proposal is that the puzzle of multiple populations remains unsolved, hence alternative theories are needed (Bastian & Lardo 2017). Nevertheless, the discrepancies between models and observations are not of the same level. In this work, we limit the comparison to the models in which nuclear processing is able to trace the most extreme chemical patterns so far found in the SG stars. Only the supermassive star model and the AGB model can, at least qualitatively, provide the proton captures on magnesium nuclei required to explain the Mg–Al anticorrelation found in a few clusters, so here we focus on the predictions of these two models.

Sufficiently large samples of data on the Mg–Al anticorrelation have been acquired only in recent times. In clusters where it is present, the Mg–Al data provide more information on the source of pollution than the standard feature of multiple populations, the O–Na anticorrelation, for the following reasons: a) proton captures on Mg nuclei are activated at higher temperatures than those on ^{16}O and ^{22}Ne nuclei (the latter reaction leading to the synthesis of Na); b) Mg and Al abundances measured in giant stars definitely reflect the initial chemistry, as in the low mass stars evolving today in GCs, these elements are not subject to any nuclear processing, not even in the central regions. In addition Mg is a key element for any scenario, because its abundance can only decrease as a result of evolution (no production is allowed), so it is a direct signature of nuclear processing in the polluters¹.

The most recent results have confirmed the early discovery that the isotopic magnesium ratios in NGC 6752 (Yong et al. 2003) do not agree with the abundance ratios pre-

dicted in the HBB models computed so far (Ventura & D’Antona 2009). On the other hand, the observed abundance ratios $^{25}\text{Mg}/^{24}\text{Mg}$ and $^{26}\text{Mg}/^{24}\text{Mg}$ are more easily achieved in the convective cores of those supermassive stars that burn hydrogen at temperatures $\simeq 75$ MK (Denissenkov & Hartwick 2014; Denissenkov et al. 2015). In principle, this suggests that the interiors of such supermassive stars are the most plausible site for the Mg nucleosynthesis producing the chemical patterns observed in GC stars. We will discuss later on the difficulties of supermassive star model.

The paper is structured as follows. We discuss the relevant observations in Section 2, and the Mg–Al nucleosynthesis and p-capture cross sections in Section 3. We examine in detail the Mg-related nucleosynthesis occurring in the models of massive AGB stars for which we have produced yields in the recent literature.

In Section 4 the theoretical predictions, based on the chemical composition of updated AGB yields, are compared with the observations of the Mg–Al trends and with the magnesium isotopic ratios of stars belonging to GCs of different mass and metallicity. We focus on the observations of the magnesium isotopes in M13 and NGC 6752, in the attempt to reproduce the relative fractions of ^{25}Mg and ^{26}Mg with respect to the total magnesium and the extension of the Mg–Al pattern. We consider the nucleosynthesis resulting from the nuclear reaction rates currently available (the LUNA compilation, Strieder et al. 2012) and we study which variations of these rates may produce full agreement with the data. We also extend the computation to the chemistry of NCG 2419, a cluster where the abundances of the individual Mg isotopes are not available, but hosting the largest observed spread (by a factor ~ 10) in the overall magnesium abundance.

In Section 5 we perform a global comparison between the model predictions and the data, and show that these AGB models, in the framework of the dilution model, are compatible both with the depletion of magnesium in the SG in clusters of different metallicity, and with the increase in helium accounting for the MS width and the HB morphology. We also discuss the results of the supermassive star models. Finally, in Section 6 we discuss that the suggested increase in the ^{25}Mg proton capture rate is plausible, and make a plea for a new experimental determination.

2 OBSERVED MG AND AL ABUNDANCES IN GCS

Early detections of star-to-star variations in Al line strength (Norris et al. 1981; Norris & Smith 1983; Cottrell & Da Costa 1981) were confirmed as being due to Al abundance variations (Drake et al. 1992; Brown & Wallerstein 1992; Norris & Da Costa 1995). The presence of a Mg–spread among GC stars was set by the pioneering investigations by Shetrone (1996a), who detected star-to-star differences in the Mg content of giant stars in M13, and by King et al. (1998), who measured extremely low Mg abundances in stars populating the sub giant branch of M92. Later works detected hints of a possible Mg–Al anti-correlations in M3 (Cavallo & Nagar 2000; Johnson et al. 2005), M13 (Cavallo & Nagar 2000; Sneden et al. 2004; Cohen & Meléndez 2005) and NGC 6752 (Gratton et al. 2001).

¹ For instance, in the AGB scenario, the abundance of sodium in SG stars depends in great part also on the effect of the second dredge up, which brings to the envelope both sodium and the neon isotopes processed in the interior. Fast p-captures on the dredged up neon contribute to increase sodium during the first phases of HBB (e.g. Ventura & D’Antona 2006). This is often forgotten in the simplified explanations attributing only the helium abundance of AGBs to the second dredge up.

A robust and quantitative confirmation of the Mg–Al anti-correlation in some GCs came with the works by Carretta et al. (2009) and Mészáros et al. (2015). Some clusters also display the presence of a Mg–Si direct correlation. Additional, recent data on Mg–Al were presented by Carretta et al. (2012a,b, 2014); Carretta (2015); Carretta et al. (2015), Gruyters et al. (2014).

We present in Table 1 a compilation of the most recent results, for the GCs with the largest statistics, reporting the extent of the magnesium, aluminium and silicon spreads detected. We also show, when available, the initial helium range for the stars in the same cluster. The latter quantity is not directly measured, but is derived from theoretical models, either applied to describe the width of the MS or the morphology of the HB. The helium range is a key indicator of the modality with which formation of SG stars took place and monitors the possible dilution with pristine gas; we will return to this point in section 6.

The largest differences between the magnesium measured in FG and SG stars, generally of the order of $\delta[\text{Mg}/\text{Fe}] \sim -0.5$, are observed in metal poor clusters, with $[\text{Fe}/\text{H}] \lesssim -2$,² in this metallicity domain we find a variety of situations, ranging from the cluster M 30, where no Mg–spread is observed and the helium spread is estimated to be within $\delta Y \simeq 0.02$ (Mucciarelli et al. 2014), to NGC 2419, a cluster harbouring a population greatly enriched in helium (Di Criscienzo et al. 2015), where an extremely large magnesium spread, $\delta[\text{Mg}/\text{Fe}] \sim -1$, is observed (Cohen & Kirby 2012; Mucciarelli et al. 2012). In the metallicity range $-2 < [\text{Fe}/\text{H}] < -1$, the only two GCs exhibiting a significant magnesium spread, of the order of $\delta[\text{Mg}/\text{Fe}] \sim -0.4$, are M 13 and NGC 2808, both commonly believed to harbor a stellar population with a very extreme chemistry, also significantly enriched in helium; conversely, no spread is observed in NGC 288, a cluster with a metallicity ($[\text{Fe}/\text{H}] = -1.3$) lower than NGC 2808 ($[\text{Fe}/\text{H}] = -1.1$), for which the helium spread was estimated to be $\delta Y = 0.015$ by Milone et al. (2014). Finally, no magnesium spread has so far been detected in GCs with $[\text{Fe}/\text{H}] > -1$.

A further information on the conditions at which the gas from which SG stars in GCs formed can be deduced by the relative distribution of the three magnesium isotopes, which are extremely sensitive to the details of the nucleosynthesis experienced. On this regard, Yong et al. (2003) studied the distribution of magnesium isotopes in giant stars of NGC 6752: the main finding was an overall magnesium spread $\delta[\text{Mg}/\text{Fe}] \sim -0.2$, with the distribution among the various isotopes ranging from $^{24}\text{Mg}:^{25}\text{Mg}:^{26}\text{Mg} = 80:10:10$, for FG stars, to $60:10:30$, for SG stars. Shetrone et al. (1996b) presented Mg data of 7 giant stars in M13, four out of which exhibited super-solar $(^{25}\text{Mg} + ^{26}\text{Mg})/^{24}\text{Mg}$ ratios. These results were confirmed and completed in a following study by Yong et al. (2006), who found that in the most contaminated M13 stars, with the lowest magnesium and the largest aluminium, the distribution among the magnesium isotopes is 48:13:40, against the corresponding ratios detected in FG stars, found

to be 78:11:11. Finally, Da Costa et al. (2013) analysed two stars in M4, finding no appreciable spread in the distribution of the magnesium isotopes, $^{24}\text{Mg}:^{25}\text{Mg}:^{26}\text{Mg} \simeq 80:06:15$ in both stars.

3 MG-AL NUCLEOSYNTHESIS

3.1 The p-capture reaction chain

The details of proton-capture nucleosynthesis by magnesium nuclei was discussed in detail by Arnould et al. (1999), Boeltzig et al. (2016) and Iliadis et al. (2011), where the interested reader can find a thorough description of the relative importance of the different reaction channels.

When $T \simeq 60 - 100$ MK the so called MgAl cycle starts. During the last decade the nuclear reactions involved in this cycle received increasing attention. In particular, the radiative captures involving $^{24,25,26}\text{Mg}$ isotopes and ^{26}Al have been deeply studied. The MgAl cycle is initiated by the $^{24}\text{Mg}(p, \gamma)^{25}\text{Al}$ reaction. ^{25}Al decays into ^{25}Mg , which may capture another proton yielding to either $^{26}\text{Al}^g$ ground state, or $^{26}\text{Al}^m$, metastable at $E_X = 228$ keV. $^{26}\text{Al}^g$ decays via β^+ with a half life of 0.7 My into the first excited state of ^{26}Mg with a subsequent γ -ray emission. On the contrary $^{26}\text{Al}^m$ β^+ decays, with a short half life of $\tau_{1/2}^m = 6.3$ s, exclusively to the ground state of ^{26}Mg . Because of this nuclear pattern the feeding probabilities of ground state and metastable isotopes have particular relevance for the understanding of magnesium nucleosynthesis in stars. The last two reactions to consider are $^{26}\text{Al}(p, \gamma)^{27}\text{Si}$ and $^{26}\text{Mg}(p, \gamma)^{27}\text{Al}$.

The slowest processes in the cycle are $^{24}\text{Mg}(p, \gamma)^{25}\text{Al}$ and $^{25}\text{Mg}(p, \gamma)^{26}\text{Al}$, which mainly determine the time scale of the Mg nucleosynthesis. From the nuclear point of view the $^{24}\text{Mg}(p, \gamma)^{25}\text{Al}$ reaction at astrophysical energies has a contribution by a low-energy resonance and a strong direct capture component dominates the resonance contribution (Trautvetter & Rolfs 1975; Powell et al. 1999; Iliadis et al. 2010). The present uncertainty of the reaction rate at the temperature of interest for the Mg nucleosynthesis is about 20%.

The rate of the $^{25}\text{Mg}(p, \gamma)^{26}\text{Al}$ reaction is characterized by several narrow resonances (Boeltzig et al. 2016, and references therein). In particular, the resonance at 92 keV is thought to be the most important for temperatures ranging from 50 to 120 MK. Recently, this resonance has been directly studied by the LUNA experiment (Limata et al. 2010; Strieder et al. 2012), providing an update of the rates of $^{25}\text{Mg}(p, \gamma)^{26}\text{Al}^g$ and $^{25}\text{Mg}(p, \gamma)^{26}\text{Al}^m$. In particular, for $50 < T < 150$ MK, the rate of the $^{25}\text{Mg}(p, \gamma)^{26}\text{Al}^m$ production was found to be 4 times higher, while the $^{25}\text{Mg}(p, \gamma)^{26}\text{Al}^g$ 20% higher than previously assumed. At $T = 100$ MK the revised total reaction rate (Straniero et al. 2013) was determined to be a factor of 2 higher than previous determinations. The uncertainty is larger than for the $^{24}\text{Mg}(p, \gamma)^{25}\text{Al}$ reaction, since there is no information about the ^{26}Al level corresponding to this resonance.

The measurements performed at LUNA suggest a stronger feeding of ^{26}Al states that predominantly decay to the isomeric state, reducing the ground state fraction (Strieder et al. 2012; Straniero et al. 2013).

² here and throughout the paper we indicate with $\delta[X/\text{Fe}]$ the difference between the abundances of element X measured in SG stars, to which we subtract the corresponding mass fraction of FG stars

Table 1. The maximum variation (SG-FG), $\delta(X)$, in magnesium, aluminium and silicon, measured in stars of different GCs, based on the number of stars N, indicated in col. 7. The helium maximum variation, δY (col. 8), is based on models reproducing the MS and/or the morphology of the HB.

name		[Fe/H]	$\delta[Mg/Fe]$	$\delta[Al/Fe]$	$\delta[Si/Fe]$	N	δY
NGC 7078	M15	-2.37	-0.50 ¹	1.10	0.40	23	0.07 ⁸
NGC 7099	M30	-2.34	0.00 ²	1.20	0.20	10	0.02 ⁹
NGC 6341	M92	-2.31	-0.60 ¹	1.10	0.30	47	
NGC 4590	M68	-2.26	-0.10 ²	1.00	0.10	13	
NGC 2419		-2.10	-1.00 ⁷	-	0.30	13	0.12 ¹⁰
NGC 5024	M53	-2.10	-0.20 ¹	1.10	0.00	16	
NGC 4833		-2.02	-0.50 ⁴	1.20	0.20	50	
NGC 5466		-1.98	0.00 ¹	0.50	0.00	3	
NGC 6809	M55	-1.93	-0.30 ²	1.00	0.00	14	
NGC 6093	M80	-1.79	-0.30 ⁵	1.30	0.10	13	
NGC 7089	M2	-1.65	-0.15 ¹	1.20	0.00	18	
NGC 1904	M79	-1.57	0.00 ²	1.00	0.00	10	
NGC 6254	M10	-1.57	0.00 ²	1.00	0.10	14	
NGC 6752		-1.55	-0.15 ²	1.20	0.20	14	0.07 ¹⁶
NGC 6205	M13	-1.53	-0.40 ¹	1.40	0.00	81	0.10 ¹¹
NGC 3201		-1.51	0.00 ²	1.00	0.00	13	
NGC 5272	M3	-1.50	-0.18 ¹	1.00	0.00	59	0.05 ¹²
NGC 6218	M12	-1.33	0.00 ²	0.50	0.00	11	
NGC 288		-1.30	0.00 ²	0.00	0.00	10	0.015 ¹³
NGC 5904	M5	-1.29	0.00 ¹	1.00	0.00	102	
NGC 6121	M4	-1.17	0.00 ²	0.00	0.10	14	
NGC 1851		-1.15	-0.08 ³	0.80	0.05	60	
NGC 2808		-1.12	-0.40 ⁶	0.00	0.10	139	0.13 ¹⁴
NGC 6171	M107	-1.02	0.00 ¹	0.70	0.00	12	
NGC 6838	M71	-0.83	0.00 ²	0.70	0.10	12	
NGC 104	47Tuc	-0.77	0.00 ²	1.00	0.00	11	0.03 ¹⁵

The references of the data on the various clusters are the following: 1 - Meszaros et al. (2015); 2 - Carretta et al. (2009); 3 - Carretta et al. (2012b); 4 - Carretta et al. (2014); 5 - Carretta et al. (2015); 6 - Carretta (2015); 7 - Carretta et al. (2014); 8 - Milone et al. (2013); Mucciarelli et al. (2014); 10 - Di Criscienzo et al. (2015); 11 - D’Antona & Caloi (2008); 12 - Caloi & D’Antona (2008); 13 - Piotto et al. (2013); 14 - D’Antona & Caloi (2013); 15 - Di Criscienzo et al. (2010); 16 - Tailo et al., in preparation

3.2 P-capture reactions on Mg isotopes in massive AGB envelopes

A series of studies showed that magnesium burning can be easily achieved in low-metallicity, massive AGB stars (Ventura et al. 2011; Ventura & D’Antona 2011; Ventura et al. 2013). The modality with which Mg-poor ejecta are produced by AGB stars is related to the ignition of HBB, a physical mechanism by which the base of the external envelope of $M \geq 4 M_{\odot}$ stars reaches temperatures above ~ 30 MK, sufficiently hot to start proton-capture nucleosynthesis (Renzini & Voli 1981; Blöcker & Schönberner 1991). The same studies showed that the activation of magnesium burning is extremely sensitive to the metallicity, much more than other channels, such as C-N and Ne-Na burning; this is due to the higher temperatures required to start ^{24}Mg burning in AGB stars (Izzard et al. 2007), of the order of $T \sim 90$ MK, and to the higher efficiency of HBB in low-metallicity AGB stars (Ventura & D’Antona 2008, 2009; Ventura et al. 2013).

The main features of the Mg-Al nucleosynthesis associated to HBB in massive AGB stars is reported in Fig. 1, showing the evolution of the surface mass fractions of the magnesium isotopes and of aluminium; the total magnesium is also shown. Fig. 1 refers to a $5 M_{\odot}$ model calculated with the metallicity of M13 ([Fe/H]=-1.5) and the same initial

magnesium of FG stars in M13, $[\text{Mg}/\text{Fe}] = +0.2$ ³, according to the recent observations by Mészáros et al. (2015); within the framework of the self-enrichment mechanism by AGB stars, it is a typical mass expected to provide the gas from which SG stars formed. Notice that in the cluster NGC 2419, the presence of SG stars largely enhanced in helium suggests pollution from more massive AGB and/or super-AGB stars ($6-8 M_{\odot}$, Ventura et al. 2013). The HBB temperatures in this case are $T \sim 100 - 150$ MK⁴.

³ This estimate is somewhat uncertain, given the large spread in the magnesium abundances among the FG stars of M13 in the data by Mészáros et al. (2015). Other works on the same cluster find a higher initial Mg, suggesting a possible offset in the data. The choice of the initial Mg does not affect the overall Mg depletion caused by HBB, because the rate of Mg burning scales linearly with the Mg mass fraction. The same holds for the relative fractions of the various isotopes, provided that the same initial ratios are used. On the other hand, Al production is influenced by the assumed initial Mg, because a higher availability of magnesium leads to higher Al production. Therefore, in the results shown in Fig. 2 and 3, the theoretical Al abundances must be considered as lower limits.

⁴ The temperature of the base of the envelope changes during the AGB phase: initially T increases as the core mass grows, whereas towards the end of the evolution T diminishes, because of the gradual loss of the external mantle. However, during the time

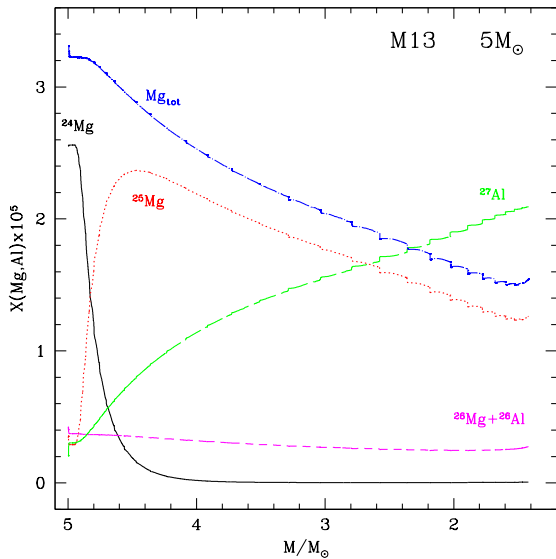


Figure 1. The evolution of the surface mass fractions of ^{24}Mg (black, solid line), ^{25}Mg (red, dotted), $^{26}\text{Mg}+^{26}\text{Al}$ (magenta, dashed), ^{27}Al (long-dashed, green) and total magnesium (dotted-dashed, blue) in a model of initial mass $5 M_{\odot}$, with the same chemical composition of stars belonging to the FG of M13. We report the (current) mass of the star on the abscissa, to have a better idea of the chemistry of the ejecta.

We see in Fig. 1 that ^{24}Mg burning starts since the initial AGB phases, leading to a significant drop in the ^{24}Mg content and to the formation of ^{25}Mg ; the latter isotope reaches a maximum and then declines. ^{26}Mg is only marginally touched by this nuclear activity, whereas ^{27}Al is produced. Despite the depletion of the overall magnesium is within a factor ~ 2 , this results in a significant increase in the aluminium content, because magnesium is much more abundant than aluminium.

A clear result from Fig. 1 is that the ejecta of these stars will be greatly enriched in ^{25}Mg ; it is indeed the accumulation of the latter isotope in the surface regions which prevents a higher depletion in the overall magnesium. The central role played by ^{25}Mg in the overall Mg-Al nucleosynthesis was underlined by Ventura et al. (2011). The large ^{25}Mg content expected in the ejecta of massive AGB stars was used by Denissenkov et al. (2015) as argument pointing against the self-enrichment by AGBs scenario.

3.3 The status of the art in modelling Mg-Al-Si in AGB envelopes

The comparisons between observations and model results are based on the assumption that the formation of SG stars occurs in gas formed by mixing of the polluters ejecta (in the present case, the AGB ejecta) with gas having the same

when most of mass loss occurs the temperature at the base of the external mantle of the stars is approximately constant, which allows us to define a typical HBB temperature.

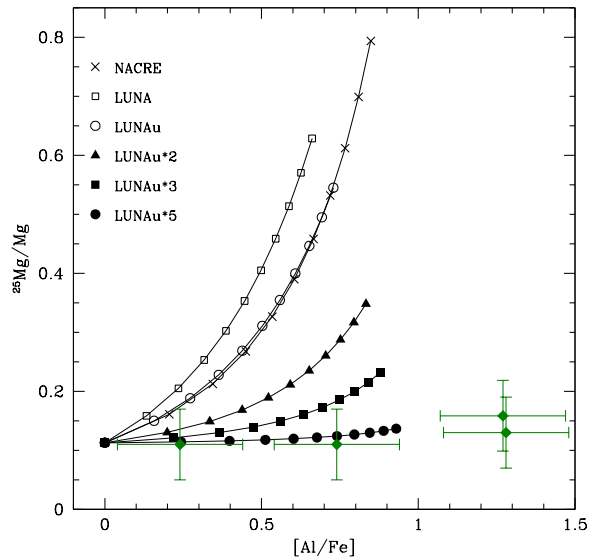


Figure 2. The fraction of ^{25}Mg with respect to the overall magnesium in the gas ejected by a $5 M_{\odot}$ AGB model, run with the chemical composition of M13 stars. The various symbols indicate the results obtained with different cross sections of the proton capture reactions by ^{25}Mg nuclei. Open circles, full triangles, squares and points indicate, respectively, the results obtained by considering the upper limits for the above reactions and the same upper limits multiplied by a factor 2, 3 and 5. The various points along a given track indicate the results obtained when mixing the pure AGB ejecta with variable percentages of gas pristine, with 10% steps. The green diamonds represent the results on M13 giants by Yong et al. (2006).

composition of FG stars (pristine gas). The ratio of polluter to pristine gas may vary from 1 (pure ejecta) to zero (pure first generation gas). This hypothesis is necessary in all formation scenarios (Decressin et al. 2007b; Denissenkov et al. 2015), as it is demanded by the shape of the correlations - anticorrelations patterns (e.g. Carretta et al. 2012a). For the AGB scenario, the model has been applied to several clusters (D’Ercole et al. 2010, 2012; Ventura et al. 2014), finding a reasonable, although certainly not perfect, correspondence between the yields and the measured abundances (D’Antona et al. 2016).

The strong nucleosynthesis activated via HBB at the bottom of the external mantle of massive AGB stars, with the extreme sensitivity of the strength of HBB to the metallicity, allowed Ventura et al. (2016) to interpret the Mg-Al trends of GC stars based on Apogee data, published in Mészáros et al. (2015), as due to self-enrichment by AGB stars belonging to the FG of the same clusters. The models presented in Ventura et al. (2016) could successfully reproduce the large Mg and Al spreads showed by M92 stars, the smaller Mg spread observed in M3 and the Mg-Al trends observed in two more metal-rich clusters, M5 (no Mg-spread, significant Al spread) and M107 (no spread in Mg and Al). The comparison with M13 data showed that the stars with the most extreme chemical composition have Mg abundances $\sim 0.15 - 0.2$ dex smaller than predicted by the AGB

models of the appropriate metallicity. The approach followed by Ventura et al. (2016) was extended to other Galactic GCs in the recent study by Dell’Agli et al. (2018).

On the wake of the results by Ventura et al. (2016) and Dell’Agli et al. (2018), we may explain the different depletion of magnesium and aluminium reported in Table 1 as due to the gas ejected by massive AGB stars, which shows a higher degree of alteration with respect to the original chemistry for lower metallicity. For GCs sharing the same metallicity, the most extended Mg-Al trends are detected in the clusters where some SG stars formed directly from genuine gas expelled by AGB stars, consistent with the large helium spread detected.

We now make a step forward towards a full and satisfactory interpretation of the chemical patterns observed in GCs, by attempting to reproduce qualitatively and quantitatively the extension of the Mg-Al anti-correlation in the GCs harbouring stars with an extreme chemistry, formed from the gas expelled from polluter stars. This analysis is more robust and complete in comparison with previous works on this argument, because we test our findings against the relative distribution of the magnesium isotopes, which is extremely sensitive to the temperature at which the gas processed by p-capture nucleosynthesis, from which SG stars formed, was exposed.

Apart from supermassive stars (see Section 6), the Hot Bottom Burning envelopes of AGBs are the only stellar p-burning environment reaching the high temperatures necessary to process ^{24}Mg (Prantzos et al. 2007), but today’s p-capture rates provide ratios of the Mg isotopes which are at variance with the available observational data. It is therefore necessary to work out whether ratios consistent with the available data can be obtained by varying the relevant cross sections. In the end, we may ask whether the required variations are compatible with the uncertainties of the cross sections determinations, and new measurements may be planned to check these predictions.

Based on the arguments given above, we will primarily focus our analysis on M13 and NGC 6752, two clusters for which isotopic ratios in stars with significantly different total magnesium abundances are available. We will also consider NGC 2419, as it is the cluster where the largest Mg spread has been detected so far. We are not discussing the results on M4 stars by Da Costa et al. (2013), because the two stars observed show a very large overall $[Mg/Fe] = +0.4$ and very similar isotopic ratios, thus suggesting that they both belong to the FG of the cluster.

4 MODEL COMPUTATION

The results regarding the Mg-Al nucleosynthesis used in the previous papers by our group, including Ventura et al. (2016) and Dell’Agli et al. (2018), have been based on the NACRE (Angulo et al. 1999) cross sections for proton capture reactions by magnesium and aluminium isotopes. To infer which is the largest depletion achievable for a given metallicity, we used the NACRE upper limits for the reaction rates of proton captures by ^{25}Mg , ^{26}Mg and ^{26}Al .

The NACRE rates have been revised and we are interested into a more detailed analysis, aimed at understanding the variation of the individual isotopes, besides the extent

of the overall depletion of magnesium. Therefore, we fully update the rates, by adopting the STARLIB library (Salaska et al. 2013), completed by the newest results from the LUNA collaboration for what attains the cross sections of the proton capture reactions by ^{25}Mg nuclei (Straniero et al. 2013).

4.1 M13

To study the Mg-Al nucleosynthesis in M13 we calculated several evolutionary sequences of the $5 M_{\odot}$ model shown in Fig. 1, with various assumptions regarding the cross sections of the proton capture reactions by the isotopes involved in the Mg-Al chain. The chemical composition is the same as given in Mészáros et al. (2015) for FG stars in M13, i.e. $[\text{Fe}/\text{H}] = -1.5$, $[\text{O}/\text{Fe}] = +0.55$, $[\text{Mg}/\text{Fe}] = +0.2$ and $[\text{Si}/\text{Fe}] = +0.4$. The mass fractions of all the other species are assumed to be solar scaled. These choices lead to the metallicity $Z = 10^{-3}$.

In Fig. 2 we show the expected variation of the $^{25}\text{Mg}/\text{Mg}$ ratio versus Al in the gas ejected; the quantities shown in the plane reflect the average chemical composition of the gas expelled by the star during the whole AGB phase. In the figure we show a dilution curve, obtained by assuming various degrees of mixing between the material lost by the star via stellar winds and pristine matter, having the same chemical composition as the FG stars in the same cluster. The observations by Yong et al. (2006) are also reported in the same plane.

The results in Fig. 2 confirm that when using the NACRE reaction rates, the Mg content of the ejecta is dominated by ^{25}Mg ($\sim 80\%$ of the total Mg). To make the fraction of ^{25}Mg compatible with the observations, i.e. $\sim 10\text{--}30\%$, we must consider a dilution with at least 70% pristine gas; this is even less compatible with the observational evidence, as the Al-enhancement would be $\delta[\text{Al}/\text{Fe}] < 0.5$. Fig. 2 also shows that adopting the recommended values, or the upper limits of the LUNA cross sections for the two proton capture reactions by ^{25}Mg , does not improve the agreement with the data.

We also plot the results obtained by artificially multiplying the LUNA cross sections by different factors. The slope of the various curves is flatter the higher are the rates adopted, owing to the lower equilibrium abundances of ^{25}Mg obtained for higher rates. The results shown in Fig. 2 indicate that, as far as the relative fraction of ^{25}Mg is concerned, the agreement with the results by Yong et al. (2006) requires that the LUNA cross sections must be increased by at least a factor 3. We note that while the results shown in Fig. 2 have been obtained by enhancing by the same factor both the ^{25}Mg burning channels, we would come to similar conclusions if we had modified solely the slower reaction giving the time scale of ^{25}Mg burning, i.e. the $^{25}\text{Mg}(p, \gamma)^{26}\text{Al}^{\text{m}}$ reaction. This follows the discussion in section 3.1.

Fig. 3 shows the relative fractions of ^{25}Mg and ^{26}Mg and the overall Mg-Al trend, for the same $5 M_{\odot}$ model discussed in the previous figures. As in Fig. 2, we focus on various combinations of cross-sections, with the LUNA rates for ^{25}Mg burning multiplied by a factor of 2 or more.

The results in Fig. 3 indicate that an ad hoc increase in the LUNA rates are not sufficient to achieve agreement between models and observations, because adopting higher

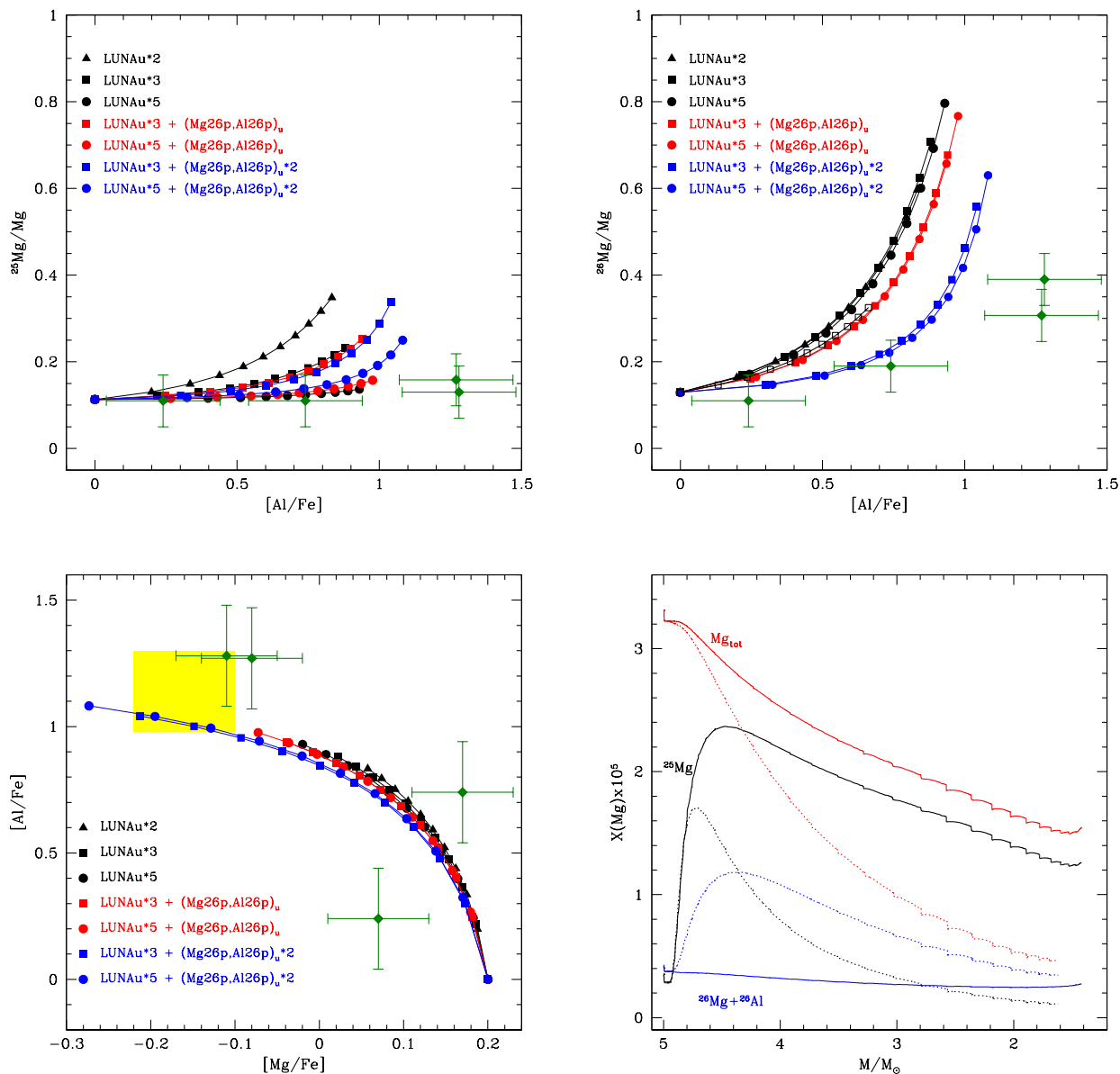


Figure 3. The relative fractions of ^{25}Mg (top, left panels) and ^{26}Mg (top, right) and of the Mg-Al mass fractions (bottom, left) in the gas lost by the $5 M_\odot$ model shown in Fig. 1, for various choices of the relevant cross-sections. We show the dilution curves, obtained by mixing the AGB gas with various fractions (from 0 to 100%, with 10% steps) of pristine matter. The results on M13 giants by Yong et al. (2006) are indicated with green diamonds. The yellow shaded region points the zone in the various planes populated by M13 stars with the most extreme chemical composition by Mészáros et al. (2015). In the bottom, right panel we report the sensitivity to the choice of the cross-sections of the evolution of the magnesium isotopes and of aluminium, for the same model described in Fig. 1: the solid tracks correspond to the results shown in Fig. 1, whereas dotted lines indicate the results obtained when adopting the same cross sections as the full, blue squares in the other panels.

rates for proton captures by ^{25}Mg nuclei, while decreasing the relative fraction of ^{25}Mg , would favour extremely large $^{26}\text{Mg}/\text{Mg} > 60\%$, at odds with the values found by Yong et al. (2006). This can be seen in the right, top panel of Fig. 3, where we note the large values attained by $^{26}\text{Mg}/\text{Mg}$ when using the enhanced LUNA rates with the recommended

STARLIB rates for proton captures by ^{26}Mg and ^{26}Al (black dots).

This problem is somewhat alleviated when the upper limits for the same reactions are adopted (red dots in the same panel), whereas the agreement is satisfactory when the cross sections of the reactions involving ^{26}Mg and ^{26}Al are multiplied by a factor of 2 (blue dots in Fig. 3).

This choice also allows fixing the problem of the overall depletion of magnesium detected in M13 stars with the most extreme chemistry, discussed in Ventura et al. (2016): this can be seen in the left, bottom panel of Fig. 3, showing that a total depletion $\delta(\text{Mg}) \sim -0.4$ is obtained when using the combination of the LUNA cross sections increased by a factor $\sim 3 - 5$ and the STARLIB rates for proton captures by ^{26}Mg and ^{26}Al enhanced by a factor 2.

In the right, bottom panel of Fig. 3 we compare the results shown in Fig. 1 with those obtained with the combinations of LUNA and STARLIB rates discussed above. We note the significant differences in the behaviour of ^{25}Mg and, as a consequence, in the overall magnesium.

4.2 NGC 6752

We tested the combination of cross sections used for M13 in the previous section against the results on the Mg and Al abundances of NGC 6752 stars by Yong et al. (2003); to this aim, we calculated AGB models with the same metallicity as M13 ($[\text{Fe}/\text{H}] = -1.5$), but with a higher initial magnesium ($[\text{Mg}/\text{Fe}] = +0.5$) than M13.

We compare the chemical composition of the ejecta from AGB stars with the observations in Fig. 4; the three panels of the figure show the dilution curve of pure AGB gas mixed with different fractions of pristine gas, with the same chemistry of FG stars.

On the Mg-Al plane, shown in the left panel of Fig. 4, the observations are well reproduced by the models. These results indicate that SG stars in this cluster formed from AGB gas mixed with pristine gas. The chemical composition of the star with the most extreme chemistry, i.e. with the largest Al and the smallest Mg, is compatible with AGB gas diluted with $\sim 40\%$ of pristine gas.

The comparison of the models with the relative fractions of ^{25}Mg and ^{26}Mg is also pretty satisfactory. The dilution curves in the middle and right panels of Fig. 4 reproduce the observed trends, with the same degree of mixing required to fit the Mg-Al trend.

The analysis of NGC 6752 stars outlines a clear difference compared to M13, because in this case a significant fraction of pristine gas (more than $\sim 30\%$) is required. It is possible that the sample we are examining (Yong et al. 2003) does not include stars with more extreme chemistry (Grundahl et al. 2002), and in fact the horizontal branch morphology of the cluster stars requires a variation (SG-FG) of helium up to $\delta Y \sim 0.07$ (Tailo et al., in preparation), while the “average” width of the MS is only $\delta Y \sim 0.04$ (Milone et al. 2013).

In the models which deplete Mg, the nucleosynthesis proceeds up to silicon. The mild correlation between Al and Si abundances found by Yong et al. (2003) can be compared with that predicted by these models. The observed $\delta[\text{Si}/\text{Fe}]$ between the abundance in models with standard Al and the average abundance in models with high Al is ~ 0.04 dex. In the ejecta of the $6M_{\odot}$ we find $\delta[\text{Si}/\text{Fe}] \sim +0.035$ dex, so for a dilution of 40% the total variation expected is $\sim +0.02$. We can regard this comparison as a reasonable agreement, in view of the large uncertainties in Silicon production and Magnesium depletion discussed in Ventura et al. (2011).

4.3 NGC 2419

NGC 2419 is a very peculiar metal-poor GC ($[\text{Fe}/\text{H}] = -2.1$, see Table 1), as witnessed by the complex morphology of the HB and the chemical patterns traced by the distribution of the observed mass fractions of some species, determined by high-resolution spectroscopy.

The analysis by Di Criscienzo et al. (2015) showed that the HB of NGC 2419 can be explained only by invoking the presence of a helium-rich population, with $Y > 0.35$. In the AGB scenario, this is consistent with the formation of SG stars directly from the winds of very massive AGB stars, the progeny of stars with initial mass above $\sim 6 M_{\odot}$. Models for the formation of an extreme SG from undiluted AGB ejecta have been proposed by D’Ercole et al. (2008, 2016) and D’Antona et al. (2016). Dilution with pristine gas, if any, must have been negligible in this case, otherwise the helium content of these SG stars would be smaller, as a consequence of mixing of helium-rich matter from the AGB winds with $Y \sim 0.25$ pristine gas.

Furthermore, the results from spectroscopy outlined the presence of an extremely large Mg-spread (Cohen & Kirby 2012) and of a clear magnesium-potassium anticorrelation (Mucciarelli et al. 2012). An interesting point on this side is that the distribution of the stars in the Mg-K plane is bimodal, with a group of stars with large Mg and solar scaled K, likely the FG of the cluster, well separated by SG stars, which exhibit a large Mg depletion ($\delta[\text{Mg}/\text{Fe}] \sim -1$ dex compared to FG stars) and K enhancement ($\delta[\text{K}/\text{Fe}] \sim +1$ dex). Ventura et al. (2012) suggested that such an extreme chemical composition could be achieved in the interior of massive, metal-poor AGB stars, owing to the effects of a very strong HBB.

The independent analysis by Iliadis et al. (2016), aimed at fixing the thermodynamic conditions compatible with the nucleosynthesis required to reproduce the most extreme chemistries of NGC 2419 stars, confirmed that the temperatures and densities achieved at the base of massive AGB models of the same metallicity of NGC 2419 can account for the chemical composition of the stars with the most extreme chemistry.

In spite of the lack of Mg isotopic ratios determinations, it is interesting to test the AGB models presented here against the Mg spread observed in NGC 2419, because an evaluation of the reliability of the theoretical description given here can be obtained by comparing the chemical composition of the ejecta of massive AGB stars with the chemistry of SG stars in the cluster. As there has been very little or no dilution with pristine gas, a direct comparison between models and observations is possible.

To this aim, we calculated massive AGB models with the metallicity of NGC 2419 stars, with the O, Mg and Si observed in FG stars of this cluster: $[\text{O}/\text{Fe}] = +0.4$, $[\text{Mg}/\text{Fe}] = +0.4$, $[\text{Si}/\text{Fe}] = +0.35$. This mixture and the assumed $[\text{Fe}/\text{H}]$ correspond to the metallicity $Z = 2 \times 10^{-4}$. The left panel of Fig. 5 shows the temporal variation of the surface chemical composition of a $7 M_{\odot}$ star, during the AGB phase. Owing to the effects of the second dredge-up, the helium content of the gas ejected by this star is $Y = 0.37$, in agreement with the analysis by Di Criscienzo et al. (2015). We focus on the surface abundance of Na, Mg, Al, Si, the only elements involved in p-capture nucleosyn-

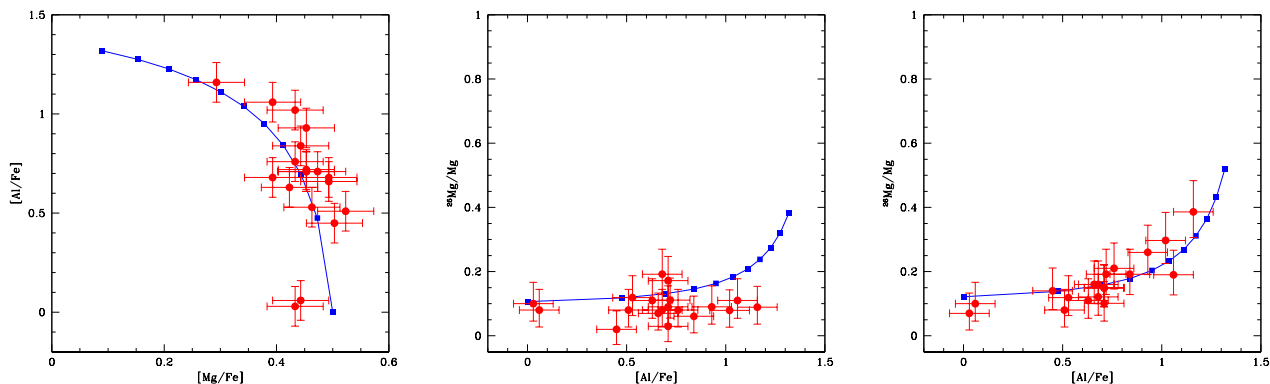


Figure 4. The observation of NGC 6752 by Yong et al. (2003) overimposed to results from AGB modelling regarding the Mg-Al abundances (left panel) and the relative fractions of ^{25}Mg (middle) and ^{26}Mg (right). As in the previous figures we show the results obtained by diluting the AGB material with pristine gas.

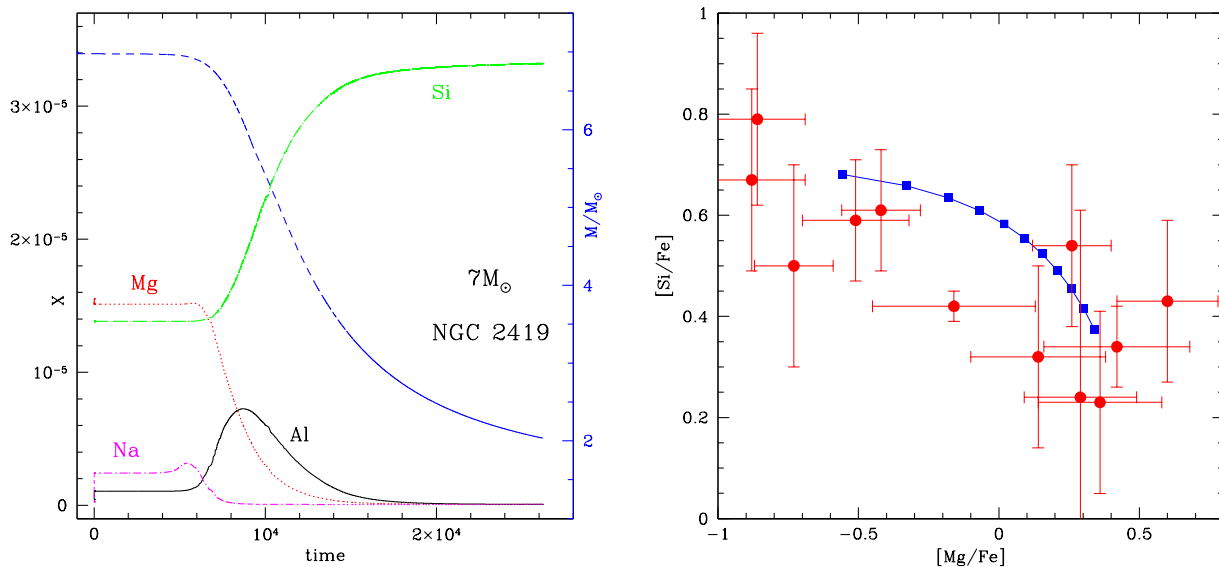


Figure 5. Left: The AGB evolution of the total magnesium (red, dotted line), aluminium (black, solid), silicon (green, dotted-dashed) and sodium (long-dashed, magenta) in a $7 M_{\odot}$ model with the same chemical composition of stars in NGC 2419. Right: The dilution pattern of the Mg-Al content in the AGB models presented in the left panel, overimposed to the observations by Cohen & Kirby (2012).

thesis for which we have data from Cohen & Kirby (2012). In the same figure we also show the evolution of the mass of the star (scale on the right), to have an idea of the chemical composition of the ejecta.

The results shown in the left panel of Fig. 5, can be summarized as follows:

(i) The overall magnesium is destroyed at base of the envelope of massive AGB stars with the metallicity of NGC 2419, via strong HBB. The destruction of magnesium begins after $\sim 20\%$ of the AGB phase has past; because during this time little mass was lost by the star, the gas ejected is magnesium-poor.

(ii) When Mg burning starts, Al-production occurs. However, owing to the very hot HBB temperatures, in later phases Al is destroyed by proton fusion, in favour of silicon. We expect only a moderate increase in Al in the gas expelled.

(iii) The combination of Mg and Al burning leads to the synthesis of silicon. The final silicon is almost a factor 3 higher than the silicon initially present in the star.

(iv) The HBB temperatures at which the base of the envelope is exposed are too large to allow the formation of great quantities of sodium. The initial increase in the surface sodium triggered by the second dredge-up and by proton capture by ^{22}Ne nuclei is followed by a phase during

which sodium is destroyed owing to proton capture. The average sodium in the gas ejected is only slightly increased with respect to the initial chemical composition.

In the right panel of Fig. 5 we show the Mg–Si observations by Cohen & Kirby (2012) compared to the chemistry of the ejecta; the results for various degrees of dilution of the pure AGB gas with pristine matter are indicated. We choose the Mg–Si plane to make this comparison, because the Al is available only for part of the stars in the Cohen & Kirby (2012) sample and no error bars are given for this element.

The overall Mg spread of the $7 M_{\odot}$ model reproduces the difference between the average Mg of FG and SG stars in NGC 2419; this is also in agreement with the main finding by Mucciarelli et al. (2012), who found a factor ~ 10 difference in the Mg of FG and SG stars. This is a further confirmation that the combination of cross sections required to fit M13 data allow to reproduce the large Mg spread shown by NGC 2419 stars.

Regarding the chemical composition of SG stars in this cluster, we note that the small Al and Na spread between FG and SG stars observed by Cohen & Kirby (2012), as also the $\delta[Si/Fe] \sim 0.3$ silicon spread, are consistent with the results summarized in the points (i)–(iv) given above.

5 GLOBAL COMPARISON WITH DATA

5.1 The AGB scenario, with the revision proposed for reaction rates

Fig. 6 shows the data of Table 1 compared with the yields of HBB in the above computations, in which the reaction rate of the proton capture reactions on ^{25}Mg has been multiplied by three and those on ^{26}Mg and ^{26}Al nuclei have been multiplied by a factor two. We plot the δMg versus δY data, assuming that the magnesium determination is affected by global errors of 0.1 dex. We do not show the indetermination in the Y values, but remember that these are derived by model interpretation of CM diagram features such as the HB and the MS width, so a fair error on the largest numbers would be at least $\delta Y = \pm 0.01$, while in the clusters where small values are found, these values are compatible with zero. The three lines correspond to dilution curves for the metallicities of the computed models. With the limit of the modelling, the figure shows two main observational trends, which provide a strong indication that indeed the AGB scenario describes correctly the chemical anomalies concerning magnesium.

(i) The Mg and helium spreads are correlated: in the clusters having a small He spread, e.g. M30 and 47Tuc, no Mg variation is detected. The largest variations are found in clusters also harboring a very helium rich population. This reflects the role of dilution: a small helium spread suggests that no He-rich stars formed, i.e. that the contaminated gas, enriched in helium, was diluted with a significant fraction of ‘pristine’ gas, whose composition is the same or close to the chemistry of the FG stars. In this interpretation, it is not surprising that no significant Mg spread is observed. If the processed Mg-poor gas lost by the polluters was mixed with Mg-rich, pristine gas, the SG stars formed will have a very small (if any) magnesium depletion. Provided that

strong dilution partly erases the effects of the nucleosynthesis, we understand that the clusters we should look at to infer the most complete and exhaustive information on the possible polluters are those exhibiting the most extended helium spread, because they likely harbor (part of) SG stars formed without any dilution, whose chemical composition reflects more directly the effects of the nucleosynthesis at which the contaminating gas was exposed. Here we also remark that such a direct correlation with the helium abundance is not expected for sodium, because the sodium yield is not a result of pure destruction in HBB, but of a complex interplay between the 2DU of sodium, the early conversion of the ^{22}Ne , acquired at the 2DU, into sodium by proton capture, and the sodium burning during HBB (Ventura & D’Antona 2006).

(ii) The data reported in Fig. 6 show a clear trend with metallicity: among the clusters harboring stars greatly enriched in helium, the Mg spread gets wider the lower is $[Fe/H]$. The cluster presenting the largest difference between the Mg measured in FG and SG stars ($\delta[Mg/Fe] \sim -1$) is NGC 2419, a metal-poor cluster ($[Fe/H] = -2.1$) in which the presence of helium rich stars was proved beyond any reasonable doubt. NGC 2808 and M13, also believed to harbor a helium-rich population, exhibit a narrower Mg spread compared to NGC 2419, i.e. $\delta[Mg/Fe] \sim -0.4$; these clusters are more metal rich than NGC 2419, thus confirming the considerable sensitivity of the Mg depletion to the iron content found in the modelling.

In the context of the AGB scenario, the trends of the extension of Mg depletion with respect to both dilution and metallicity displayed in Fig. 6 apply also to the less explored elements silicon and potassium. In particular, the recent results concerning the K dispersion (Mucciarelli et al. 2017) are in perfect agreement with this scenario.

5.2 The supermassive star models

The data and this new modelling offer a valuable opportunity to discriminate among the various polluters that might have produced the gas from which SG stars formed in GCs. A successful model is required to produce advanced Mg–Al nucleosynthesis during H–burning, so to produce Mg-poor, He-rich material, *in a modality strongly sensitive to metallicity*.

This evidence seems to indicate that massive binaries and fast rotating massive stars could hardly have played a role in this context, because the core temperatures of these stars during core hydrogen burning, mainly determined by hydrostatic conditions requirements, thus scarcely sensitive to the details of stellar modelling, are not sufficient to start Mg proton captures, and to produce gas with a Mg content comparable to the one observed in the most metal poor GCs, such as NGC 2419 (see the detailed discussion in section 2.2 in D’Antona et al. (2016)).

In section 4 we showed that the yields of massive AGB models can account for the observational evidence, being able to reproduce the Mg spread observed in M13 and NGC 2419, and its trend with metallicity. However the observations of the magnesium isotopes, in the few clusters where these have been observed so far, are consistent with AGB

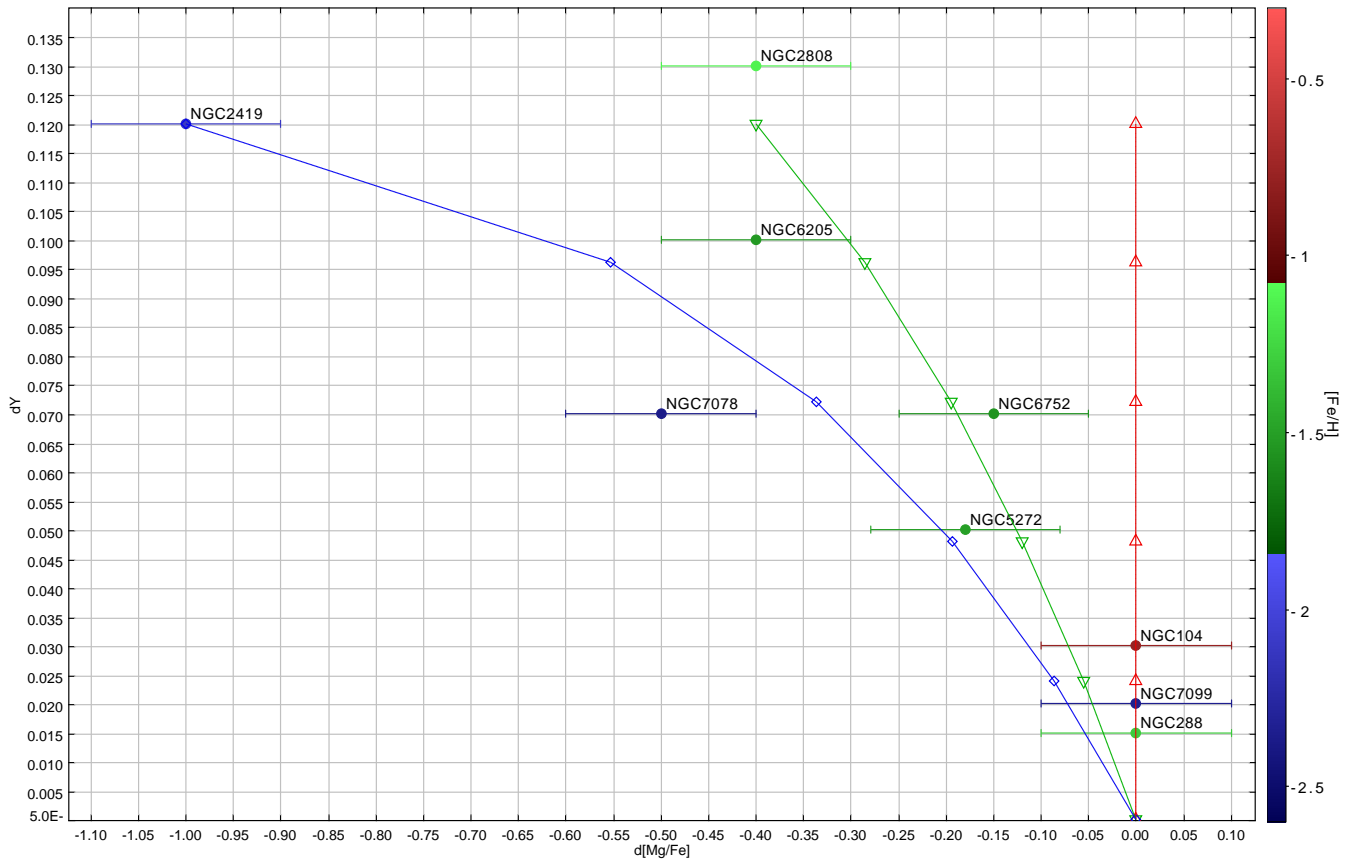


Figure 6. The magnesium and helium spread for the clusters reported in Table 1, for which the helium spread has been estimated. The colour coding corresponds to different metallicities, as reported on the right, vertical axis. The dilution curves were obtained by mixing the AGB ejecta with various percentages of pristine gas for the metallicities $[Fe/H] = -0.77$ (red), $[Fe/H] = -1.12$ (green) and $[Fe/H] = -2.1$ (blue).

yields only if the rates of the ^{25}Mg and ^{26}Mg p-captures are enhanced above the formal determination boundaries.

On the contrary, processing in the cores of supermassive stars with masses of the order of $\sim 10^4 M_{\odot}$ make a good job in reproducing the depletion and isotopic ratios *without any cross section adjustment*. Thus the supermassive stars scenario (Denissenkov & Hartwick 2014), on these grounds, looks like it can be better than the AGB scenario. Denissenkov & Hartwick (2014) show that masses $\sim 10^4 M_{\odot}$ reach core temperatures of the order of $\sim 70 - 80$ MK, sufficiently hot to activate proton capture reactions by magnesium nuclei (notice, anyway, that their results are in qualitative agreement with the observations of M13 stars, but no dilution must occur to reproduce the overall Mg depletion, while the fit of the magnesium isotopes demands $\sim 30\%$ of pristine matter). The proposers of the model, anyway, need two basic, ad hoc, hypotheses to reach a consistent result with the GC data:

- 1) The hypothetical formation of supermassive stars in GCs must be in a limited range of initial masses, around $10^4 M_{\odot}$, so that their central temperatures fall in the required range $70-80$ MK;

- 2) The maximum helium enhancement found in SG stars is $Y \lesssim 0.4$. So it is necessary that the core H-burning of such extreme objects ends at a phase when the H content

was reduced only by $\Delta X \sim 0.15$. The authors suggest that this is justified by the very unstable hydrostatic equilibrium of these hypothetical structures.

Apart from these two strong ad hoc choices, it is not clear whether these models can explain the ~ 1 dex spread in the magnesium content observed in metal-poor clusters such as NGC 2419. The trend with the metallicity is not obvious in this case, as the temperature at which nuclear activity takes place in the central regions is almost unaffected by the metallicity, unlike the HBB conditions in massive AGB stars.

6 FINAL REMARKS

Among the various species involved in the chemical patterns traced by stars in GCs, magnesium is the key-element, providing the most valuable information regarding the nature of the polluters, which released into the intra-cluster medium the gas from which SG stars formed. This is because unlike other species, such as sodium and oxygen, magnesium is not affected by any mixing episode connecting the external, convective regions of the stars with deep layers, where nuclear activity occurred; this holds both for deep mixing during the red giant branch evolution, which might alter the interpre-

tation of the observed chemical composition, and also for the second dredge-up in the progenitor AGB stars, which changes the surface chemistry before the thermal pulses phase begins. The magnesium content reflects the conditions at which the processed gas was exposed, which determine the extent of the nucleosynthesis experienced. Furthermore, unlike e.g. sodium and aluminium, the overall magnesium decreases steadily during any p-capture nucleosynthesis process, which makes the analysis more straightforward, as there is no need to consider balance between production and destruction channels, whose trend with the temperature might be not obvious. Finally, magnesium burning requires higher temperatures compared to other reactions channels, such as oxygen burning and the activation of the Ne-Na chain, which restricts the identification of the nature of the possible polluters.

Concerning the nuclear processes, in section 3.1 we have discussed the present status of uncertainties for the reactions involved in the Mg-Al chains. On the other hand we have shown that reproducing the observed isotopic ratios and the overall magnesium spread observed in clusters of different metallicity requires 3 times higher values of the $^{25}\text{Mg}(p, \gamma)^{26}\text{Al}^m$ reaction, which is larger than the uncertainty quoted by LUNA (Straniero et al. 2013).

At the temperatures ~ 100 MK, relevant for the models studied in this work, this process is dominated by the resonance at 92 keV. Most of the uncertainty in the reaction rate is due to the absence of information about the ^{26}Al level corresponding to this resonance. In particular, a key parameter to determine the rate is the ground state feeding factor (f_0) for this ^{26}Al state. In fact, as mentioned previously, the $^{25}\text{Mg}(p, \gamma)^{26}\text{Al}$ resonances decay through complex γ -ray cascades either to the 5^+ ground state or the 0^+ isomeric state at $E_X = 228$ keV.

For all the resonances at energies higher than 92 keV, f_0 can be experimentally determined, deducing level branchings from γ -ray detection. This is not possible for the resonance at 92 keV, because of its weakness. For this resonance the value of f_0 relies mainly on literature information. To our knowledge the main source to get this information is the nuclear compilation by Endt et al. (1988). Unfortunately, for the 92 keV resonance there is no clear experimental information, while for the other levels, also for those at lower energy, i.e. $E = 37$ and 57 keV, the f_0 , the determination is well grounded. This is maybe due to the fact that literature information in the case of the 92 keV resonance is contradictory. In fact, a f_0 of about 80% was deduced in Champagne et al. (1983a) and Champagne et al. (1983b). However, the same authors quote a lower value of 61% in Champagne et al. (1986). Finally, the compilation by Endt & Rolfs (1987) gives 85%. The origin of this large discrepancy is unknown, it may be possibly attributed to different assumptions on the secondary branching ratios.

In Strieder et al. (2012) specific primary γ -ray transitions from the 92 keV resonance were not identified, as they used a high efficiency 4π BGO summing crystal with a limited energy resolution. They adopted a ground-state feeding factor of $f_0 = 60^{+20}_{-10}\%$, taking into account simulations of their experimental results and the literature data. The uncertainty of the f_0 for this level now sets a limit on the reliability of estimates of the $^{25}\text{Mg}(p, \gamma)^{26}\text{Al}$ reaction in the critical temperature range.

This paper shows that measuring again this feeding factor is important to reduce the uncertainty in this cross section, relevant to the issue of the magnesium and isotopic ratios observed in the second generation of GCs.

REFERENCES

- Angulo C., Arnould M., Rayet M., et al. 1999, *Nuclear Physics A*, 656, 3
- Arnould M., Goriely S., Jorissen A. 1999, *A&A*, 347, 572
- Bastian, N., & Lardo, C. 2017, arXiv:1712.01286
- Bedin L. R., Piotto G., Anderson J., Cassisi S., King I. R., Momany Y., Carraro G. 2004, *ApJ*, 605, L125
- Blöcker T., Schönberner D., 1991, *A&A*, 244, L43
- Boeltzig A., Bruno C. G., Cavanna F., et al. 2016, *European Physical Journal A*, 52, 75
- Brown J. A., & Wallerstein G. 1992, *AJ*, 104, 1818
- Caloi V., D’Antona F. 2005, *A&A*, 435, 987
- Caloi V., D’Antona F. 2007, *A&A*, 463, 949
- Caloi V., D’Antona F. 2008, *ApJ*, 673, 847
- Carretta E., Bragaglia A., Gratton R., Lucatello S. 2009, *A&A*, 505, 139
- Carretta E., Bragaglia A., Gratton R. G., Lucatello S., D’Orazi V. 2012a, *ApJL*, 750, L14
- Carretta E., D’Orazi V., Gratton R. G., Lucatello S. 2012b, *A&A*, 543, A117
- Carretta E., Bragaglia A., Gratton R. G., et al. 2014, *A&A*, 564, A60
- Carretta E. 2015, *ApJ*, 810, 148
- Carretta E., Bragaglia A., Gratton R. G., et al. 2015, *A&A*, 578, A116
- Cavallo R. M., Nagar, N. M. 2000, *AJ*, 120, 1364
- Champagne A. E., Howard A. J., Parker P. D. 1983a, *Nucl. Ph. A*, 402, 159
- Champagne A. E., Howard, A. J., Parker P. D. 1983b, *Nucl. Ph. A*, 402, 179
- Champagne A. E., McDonald A. B., Wang T. F., et al. 1986, *Nucl. Ph. A*, 451, 498.
- Cohen J. G., Kirby E. N: 2012, *ApJ*, 760, 86
- Cohen J. G., Meléndez J. 2005, *AJ*, 129, 303
- Cottrell P. L., Da Costa G. S. 1981, *ApJL*, 245, L79
- Da Costa G. S., Norris J. E., Yong D. 2013, *ApJ*, 769, 8
- D’Antona F., Caloi V., Montalbán J., Ventura P., Gratton R. 2002, *A&A*, 395, 69
- D’Antona F., Caloi V. 2004, *ApJ*, 611, 871
- D’Antona F., Bellazzini M., Caloi V., Fusi Pecci F., Galletti S., Rood R. T. 2005, *ApJ*, 631, 868
- D’Antona F., Caloi, V. 2008, *MNRAS*, 390, 693
- D’Antona F., Vesperini E., D’Ercole A., Ventura P., Milone A. P., Marino A. F., Tailo M. 2016, *MNRAS*, 458, 2122
- De Mink S. E., Pols O. R., Langer N., Izzard R. G., 2009, *A&A*, 507, L1
- Decressin T., Meynet G., Charbonnel C., Prantzos N., Ekström S. 2007a, *A&A*, 464, 1029
- Decressin, T., Charbonnel, C., & Meynet, G. 2007, *A&A*, 475, 859
- Dell’Agli F., García-Hernández D. A., Ventura P., et al. 2018, *MNRAS*, 475, 3098
- Denissenkov P. A., Hartwick, F. D. A. 2014, *MNRAS*, 437, L21

- Denissenkov P. A., VandenBerg D. A., Hartwick, F. D. A., Herwig F., Weiss A., Paxton B. 2015, MNRAS, 448, 3314
- D'Ercole A., Vesperini E., D'Antona F., McMillan S. L. W., Recchi, S. 2008, MNRAS, 391, 825
- D'Ercole, A., D'Antona, F., Ventura, P., Vesperini, E., & McMillan, S. L. W. 2010, MNRAS, 407, 854
- D'Ercole, A., D'Antona, F., Carini, R., Vesperini, E., & Ventura, P. 2012, MNRAS, 423, 1521
- D'Ercole, A., D'Antona, F., & Vesperini, E. 2016, MNRAS, 461, 4088
- Di Criscienzo M., Ventura P., D'Antona F., Milone A., Piotto G. 2010, MNRAS, 408, 999
- Di Criscienzo M., D'Antona F., Milone A. P., Ventura P., Caloi V., Carini R., D'Ercole A., Vesperini E., Piotto G. 2011, MNRAS, 414, 3381
- Di Criscienzo M., Tailo M., Milone A. P., D'Antona F., Ventura P., Dotter A., Brocato E. 2015, MNRAS, 446, 1469
- Drake J. J., Smith V. V., Suntzeff, N. B. 1992, ApJL, 395, L95
- Endt P. M., De Wit P., Alderliesten C. 1988, Nucl. Phys. A, 476, 333
- Gratton R. G., Bonifacio P., Bragaglia A., et al. 2001, A&A, 369, 87
- Gratton R. G., Carretta E., Bragaglia A. 2012, A&AR, 20, 50
- Grundahl, F., Briley, M., Nissen, P. E., & Feltzing, S. 2002, A&A, 385, L14
- Gruyters P., Nordlander T., Korn A. J. 2014, A&A, 567, A72
- Iliadis C., Longland R., Champagne, A. E., Coc A., Fitzgerald R. 2010, Nucl. Phys. A, 841, 31
- Iliadis C., Champagne A., Chieffi A., Limongi M. 2011, ApJS, 193, 16
- Iliadis C., Karakas A. I., Prantzos N., Lattanzio J. C., Doherty, C. L. 2016, ApJ, 818, 98
- Izzard R. G., Lugaro M., Karakas A. I., Iliadis C., van Raai, M. 2007, A&A, 466, 641
- Johnson C. I., Kraft R. P., Pilachowski C. A., et al. 2005, PASP, 117, 1308
- King J. R., Stephens A., Boesgaard A. M., Deliyannis C. 1998, AJ, 115, 666
- Kraft R. P. 1994, PASP, 106, 553
- Krause M., Charbonnel C., Decressin T., Meynet G., Prantzos N. 2013, A&A, 552, A121
- Limata A., et al. 2010, Phys. Rev. C 82, 15801 ApJ, 652, 85
- Mészáros S., Martell S. L., Shetrone M., et al. 2015, AJ, 149, 153
- Milone A. P., Marino A. F., Piotto G., et al. 2013, ApJ, 767, 120
- Milone A. P., Marino A. F., Dotter A., et al. 2014, ApJ, 785, 21
- Milone A. P., Piotto G., Renzini A., et al. 2017, MNRAS, 464, 3636
- Mucciarelli A., Bellazzini M., Ibata R., Merle T., Chapman S. C., Dalessandro E., Sollima A. 2012, ApJ, 426, 2889
- Mucciarelli A., Lovisi L., Lanzoni B., Ferraro, F. R. 2014, ApJ, 786, 14
- Mucciarelli A., Merle T., Bellazzini M. 2017, A&A, 600, A104
- Norris J., Cottrell P. L., Freeman K. C., Da Costa G. S. 1981, ApJ, 244, 205
- Norris J. E., Da Costa G. S. 1995, ApJL, 441, L81
- Norris J., Smith G. H. 1983, ApJ, 272, 635
- Piotto G., Bedin L. R., Anderson J., et al. 2007, ApJL, 661, L53
- Piotto G., Milone A. P., Bedin L. R., et al. 2015, AJ, 149, 91
- Powell D. C., Iliadis C., Champagne A. E., Grossmann C. A., Hale S. E., Hansper V. Y., McLean L. K. 1999, Nucl. Phys. A 660, 349
- Prantzos N., Charbonnel C., Iliadis, C. 2007, A&A, 470, 179
- Renzini A., Voli M., 1981, A&A, 94, 175
- Renzini A., D'Antona F., Cassisi S., et al. 2015, MNRAS, 454, 4197
- Sallaska A. L., Iliadis C., Champagne A. E., Goriely S., Starrfield S., Timmes F. 2013, ApJS, 207, 18
- Shetrone M. D. 1996a, AJ, 112, 1517
- Shetrone M. D. 1996b, AJ, 112, 2639
- Snedden C., Kraft R. P., Guhathakurta P., Peterson R. C., Fulbright, J. P. 2004, AJ, 127, 2162
- Straniero O., Imbriani G., Strieder F., et al. 2013, ApJ, 763, 100
- Strieder F., Limata B., Formicola A., et al. 2012, PhLB, 707, 60
- Trautvetter H. P., Rolfs C., 1975, Nucl. Phys. A 242, 519.
- Ventura P., D'Antona F. 2006, A&A, 457, 995
- Ventura P., D'Antona F. 2008, MNRAS, 385, 2034
- Ventura P., & D'Antona F. 2009, A&A, 499, 835
- Ventura P., Carini R., D'Antona F. 2011, MNRAS, 415, 3865
- Ventura, P., & D'Antona, F. 2011, MNRAS, 410, 2760
- Ventura P., D'Antona F., Di Criscienzo M., Carini R., D'Ercole A., Vesperini E. 2012, ApJL, 761, L30
- Ventura P., Di Criscienzo M., Carini R., D'Antona F., 2013, MNRAS, 431, 3642
- Ventura, P., di Criscienzo, M., D'Antona, F., et al. 2014, MNRAS, 437, 3274
- Ventura P., García-Hernández D. A., Dell'Agli F., et al. 2016, ApJL, 831, L17
- Ventura P., Zepieri A., Mazzitelli I., D'Antona F., 1998, A&A, 334, 953
- Yong D., Grundahl F., Lambert D. L., Nissen P. E., Shetrone M. D. 2003, A&A, 402, 985
- Yong D., Aoki W., Lambert D. L. 2006, ApJ, 638, 1018